NUKLEONIKA 2004;49(Supplement 3):S37–S42

Spin and lattice dynamics of $La_{2/3}Ca_{1/3}MnO_3$ doped with 1% ^{119}Sn

**Janusz Przewoźnik,
Jan Żukrowski,
Janusz Chmist,
Ewa Japa,
Andrzej Kołodziejczyk,
Karol Krop,
Karl Kellner,
Gerhard Gritzner**

Abstract 1 at.% ^{119}Sn doped $La_{0.67}Ca_{0.33}MnO_3$ compound was studied by Mössbauer spectroscopy, magnetization, AC susceptibility and resistivity measurements. Huge separation (66 K) of the transition temperatures from the ferromagnetic (FM) to paramagnetic (PM) state (T_C) and from metallic to insulating state ($T_{M\text{-}I}$) clearly shows that transition from FM metallic to PM insulator phase goes via FM insulator phase. The Mn lattice dynamics was studied by the relative changes of Lamb-Mössbauer factor f as a function of temperature. In the Debye approximation from the calculated $-\ln(f/f_0)$ values of the characteristic Debye temperatures (θ_D) were estimated for the FM (368(10) K) and PM (391(6) K) phases. No anomaly of $-\ln(f/f_0)$ at $T_{M\text{-}I}$ and its rather spurious increase around T_C was found. The ^{119}Sn isotope as a local diamagnetic probe samples the transferred hyperfine field (B_{hf}) from its neighbour Mn magnetic moments and witnesses the dynamics of the Mn moments. Theoretical curve based on the molecular field theory was fitted to the experimental values of B_{hf}^{max} and the value of the ordering temperature ($T_C^* \approx 280$ K) of Mn moments inside the large FM domains was estimated. It is much higher than the T_C (172 K) obtained from magnetization measurement. The coexistence of FM and PM phases, which is evident from the shape of our ^{119}Sn Mössbauer spectra, was confirmed for temperatures $T \geq 150$ K and indicates the inhomogeneous character of the magnetic transition.

Key words ^{119}Sn Mössbauer • LCMO manganites • f-factor • metal-insulator

J. Przewoźnik✉, J. Żukrowski, J. Chmist, E. Japa,
A. Kołodziejczyk, K. Krop
Department of Solid State Physics,
Faculty of Physics and Applied Computer Science,
AGH University of Science and Technology,
30 A. Mickiewicza Ave., 30-059 Kraków, Poland,
Tel.: +48 12/ 617 36 07, Fax: +48 12/ 634 12 47,
e-mail: januszp@uci.agh.edu.pl

K. Kellner, G. Gritzner
Institut für Chemische Technologie Anorganischer Stoffe,
J. Kepler Universität Linz,
A-4040 Linz, Austria

Received: 9 June 2004, Accepted: 23 July 2004

Introduction

The optimally doped colossal magnetoresistance (CMR) perovskite $La_{0.67}Ca_{0.33}MnO_3$ exhibits the first-order metal-insulator (M-I) and FM-PM transitions at very close temperatures $T_{M\text{-}I}$ and T_C, respectively. The CMR response is produced around these temperatures. Although the double-exchange (DE) model [13] provides a qualitatively correct description of these materials, more complex mechanisms such as charge localization with polaron formation and phase separation have been proposed [4]. The existence of the local lattice distortion due to polarons has been experimentally documented by neutron diffraction [5], extended X-ray absorption fine structure (EXAFS) [2] and atomic pair distribution function determined by high-energy X-ray powder diffraction [1]. These studies demonstrated that atomic disorder, measured as the Mn-O bond-length distribution (increase of the Mn and O Debye-Waller factors), anomalously increases when approaching the $T_{M\text{-}I}$ (T_C) temperature. Similar conclusion was also inferred from ^{57}Fe emission Mössbauer study of $La_{0.8}Ca_{0.2}MnO_3$ compound [3]. Our earlier Mössbauer study of $(La_{0.67}Ca_{0.33})(Mn_{1-x}{}^{57}Fe_x)O_3$ compounds were not conclusive about the existence of an anomaly in the Lamb-Mössbauer factors f at $T_{M\text{-}I}$ (T_C) temperature [14]. The aim of our present study was to use ^{119}Sn Mössbauer spectroscopy to study the Mn spin and lattice dynamics in

the $La_{0.67}Ca_{0.33}MnO_3$ doped with 1 at.% ^{119}Sn. The Sn-doping into Mn sublattice replaces exclusively Mn^{4+} by Sn^{4+} [12]. The main point of our studies was to follow microscopically the evolution of the phases that appear as the temperature is varied and to determine how the relative Lamb-Mössbauer factor f changes with temperature, especially when crossing the $T_{M\text{-}I}$ temperature.

Experimental

Two polycrystalline samples of $(La_{0.67}Ca_{0.33})(Mn_{0.99}{}^{119}Sn_{0.01})O_3$ were prepared by the same sol-gel method. The first sample (denoted by #1) was sintered in air at 1400°C for 20 h but the second one (#2) at 1450°C for 50 h. The higher sintering temperature was proved to be necessary to completely dissolve 1 at.% ^{119}Sn in $La_{0.67}Ca_{0.33}MnO_3$ compound. The X-ray diffraction (XRD) patterns were collected with a D5000 Siemens diffractometer (using Cu K_α radiation and a graphite secondary monochromator) from 12° to 120° in steps of 0.02° in 2Θ and 12 s per step. The refinement of the XRD patterns was carried out by the FULLPROF program [11] assuming the perovskite $GdFeO_3$-type structure and using orthorhombic Pbnm space group. Magnetic characterization of the samples was performed on a conventional AC susceptometer and a DC VSM magnetometer. The temperature dependence of resistivity R was measured by the standard four probe method at zero external field during cooling the sample. The ^{119}Sn Mössbauer effect measurements were performed in the transmission geometry using a constant acceleration type spectrometer and $Ba^{119}SnO_3$ as the source. The temperature of the absorber was stabilized in a cryodyne refrigeration system with an accuracy better than ±0.1 K.

Results

A part of Rietveld refined X-ray diffraction pattern of the $(La_{0.67}Ca_{0.33})(Mn_{0.99}{}^{119}Sn_{0.01})O_3$ sample #2 measured at room temperature is seen in Fig. 1. Vertical arrow indicates the largest peak of the CaO impurity phase with the refined volume contribution equal to 0.97(8)%. No other impurity phases were identified. The main phase can be characterized by the following unit cell parameters a = 5.4910(3) Å, b = 5.4791(3) Å and c = 7.7452(4) Å. Our preliminary attempts to introduce larger amounts of Sn (3–6%) into $(La_{0.67}Ca_{0.33})MnO_3$ compound showed that the excess tin forms an unidentified impurity phase with the most intense peak at about 30.6 deg. To prove this possibility, the 28.5–31.5 deg. range was additionally remeasured with much longer times (90 s) per step, but no additional peak was revealed (inset in Fig. 1). Sample #1 showed a very similar XRD pattern, quite identical unit cell parameters and volume, but had clearly broader peaks in XRD pattern.

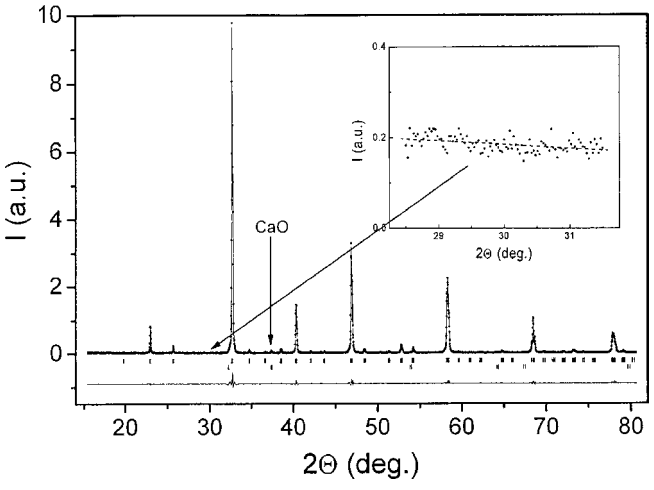

Fig. 1. Part of XRD pattern of the sample #2 at room temperature. Arrow indicates the largest peak of the CaO impurity phase. The inset shows enlarged part of the pattern measured with much better statistics.

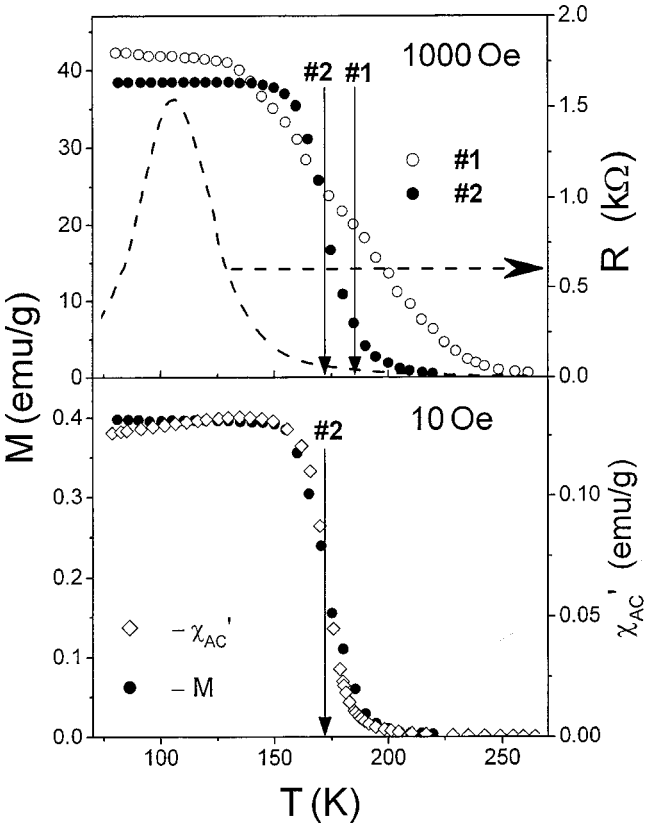

Fig. 2. Temperature dependence of magnetization for samples #1, #2 (H = 1000 Oe) and resistivity (H = 0) for sample #2 (upper panel). Lower panel shows temperature dependence of magnetization (●) in an applied magnetic field of 10 Oe and χ_{AC}' (◇) for sample #2. Vertical arrows indicate T_C values.

Measurements performed on the DC magnetometer in applied field of 1000 Oe and using a zero-field-cooling condition showed a much sharper transition from the PM to FM state for sample #2 than for sample #1. Upper panel of Fig. 2 displays magnetization for both samples and resistivity for sample #2 as a function of temperature. The typically defined T_C values (as the temperature corresponding to the minimum of dM/dT) are approximately equal to 185 K and 172 K for samples #1 and #2, respectively. The resistivity curve for sample #2 displays quite a sharp metal-isolator transition at temperature $T_{M\text{-}I}$ ≈ 106 K (defined as the maximum in R(T) curve). One should note a huge difference of about 66 K between T_C and $T_{M\text{-}I}$ temperatures for sample #2. Lower part of Fig. 2 shows the low field (10 Oe) magnetization M(T) and AC

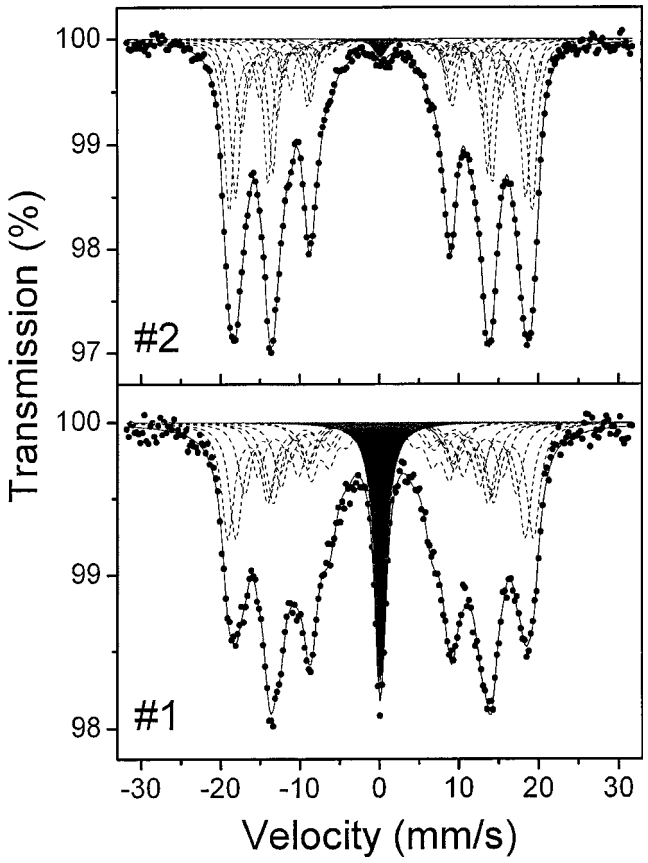

Fig. 3. Mössbauer spectra at 80 K for samples #1 (upper) and #2 (lower panel). Solid lines denote the best fits and shaded areas denote the contribution of the paramagnetic impurity phase.

susceptibility points for sample #2. The T_C value, equal to 172 K, was obtained from M(T) curve. One can note a close resemblance of the low/high field M(T) and χ_{AC}'(T) dependences. Also T_C temperatures determined in low and high magnetic field are practically the same.

To detect paramagnetic impurity phase, the Mössbauer spectra for samples #1 and #2 were recorded at 80 K. The fitted spectra are shown in Fig. 3. One can note that even minute amounts of the PM phase, denoted by shaded areas, could be detected. From the spectra of samples #1 and #2 PM, contributions of about 9.6(3)% and 0.9(2)% were found, respectively. In the fitting program, the PM phase was fitted by a single Lorentzian line and the magnetic part by many (8 or 10) sextets to take into account clear broadening and asymmetry of lines in the spectra. It is seen from these results and Fig. 3 that sample #2, sintered for a longer time (50 h) and at a higher temperature (1450°C) is a single phase and shows a better quality of Mössbauer spectra with narrower lines and from this point on, only the results obtained for sample #2 will be discussed.

The temperature evolution of selected Mössbauer spectra for $(La_{0.67}Ca_{0.33})(Mn_{0.99}{}^{119}Sn_{0.01})O_3$ compound is shown in Fig. 4. The six-line spectrum measured at 15 K for the FM state shows clear broadening and strong asymmetry of all lines, indicating that some static distribution of the values of the effective magnetic hyperfine fields B_{hf} on the ^{119}Sn nuclei exists even at 15 K. With increasing temperature gradual broadening of the six-line pattern is seen, what implies an increase of the span of the distribution of B_{hf} with an accompanying decrease of its mean value $\langle B_{hf} \rangle$. Finally, the spectrum collapses to the seemingly single line (in fact non resolved quadrupole doublet) at 200 K for the paramagnetic state. This single "paramagnetic" line appears to be seen for temperatures equal or higher than 150 K. To determine the temperature evolution of the Lamb-Mössbauer factor f, the spectra were fitted by an arbitrary number of magnetic sextets (up to 11) and a paramagnetic line with main intention to reproduce very well the shape of Mössbauer spectrum. The value of f factor for a given spectrum was calculated by summing up the values obtained for all its components ($f = \Sigma f_i$). To take into account the effect of absorber effective thickness, the program based on the transmission integral method was used. All Mössbauer spectra presented in Figs. 3 and 4 were fitted using this method. In all fits for $T < T_C$, common values of the electric quadrupole interaction parameter QS and isomer shift IS parameter were assumed for all magnetic components. In all fits, a source line half width Γ_s = 0.20 mm/s was assumed, but the absorber Γ_a values were fitted. The practically zero values of QS parameter were revealed from these fits. For each spectrum the $-\ln(f/f_0)$ parameter was calculated, where f_0 denotes the f value at 15 K. It has the sense of the mean square displacement (msd) difference ($\langle u^2 \rangle - \langle u_0^2 \rangle$) where $\langle u_0^2 \rangle$ denotes the msd of ^{119}Sn atom corresponding to f_0. The temperature

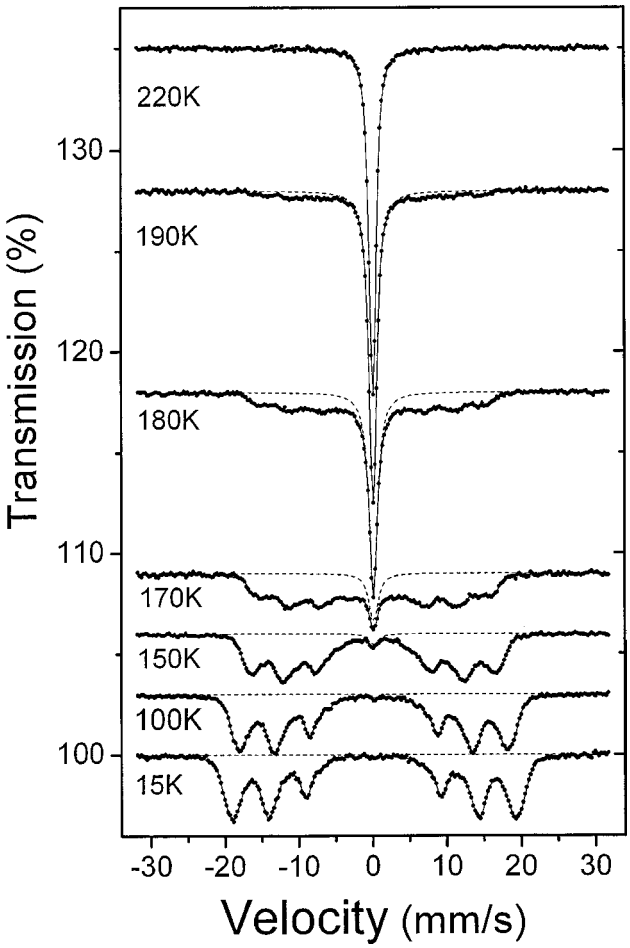

Fig. 4. Temperature variation of the selected Mössbauer spectra. Solid lines denote the fits and dashed lines fitted contribution of paramagnetic phase.

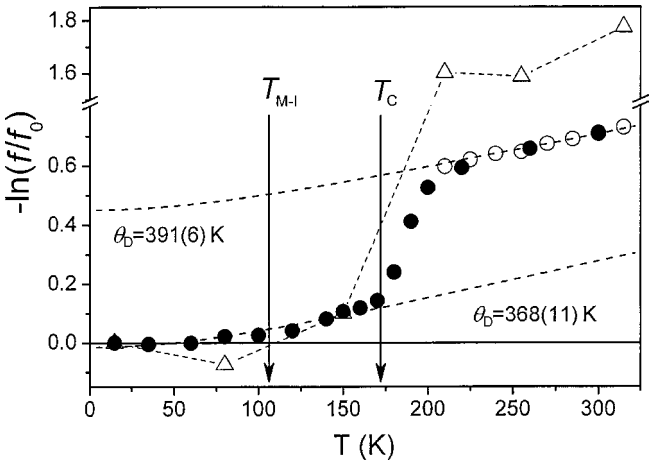

Fig. 5. Temperature variation of the $-\ln(f/f_0)$ parameter.

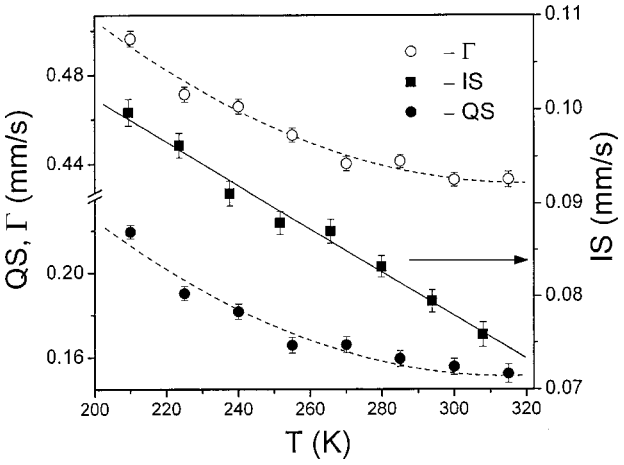

Fig. 6. Temperature variation of the quadrupole splitting QS, half line width Γ and isomer shift IS parameters. Dashed curves are to guide the eyes. Solid line was fitted to experimental points.

dependence of the $-\ln(f/f_0)$ parameter for all measured spectra is presented in Fig. 5.

Assuming the simple Debye model for the vibrational modes of the crystal one can express the f factor by the formula:

$$f = \exp\left\{-\frac{3E_\gamma^2}{mc^2 k_B \theta_D}\left[\frac{1}{4}+\left(\frac{T}{\theta_D}\right)^2 \int_0^{\frac{\theta_D}{T}} \frac{xdx}{\left(e^x-1\right)}\right]\right\},$$

where E_γ is the resonance energy and θ_D is the Debye characteristic temperature. By fitting this formula to the experimental points for the FM (denoted by ● symbol between 15 and 160 K) and PM (points denoted by ○ symbol correspond to the collapsed into single line PM spectra which were measured for smaller maximal velocity equal to 10.012 mm/s) states separately one obtains θ_D values for these two states. The fitted curves (dashed lines) together with the corresponding θ_D values are presented in Fig. 5. It can be seen that the FM state has a slightly lower θ_D temperature than the PM one and that a huge shift exists between both curves. To explain the shift between FM and PM curves, the points denoted by △ symbol were added to Fig. 5. For these selected points, the f and f_0 values were calculated in a thin absorbent limit neglecting the effect of absorber thickness. This was done to emphasize the importance of this correction especially for the PM state. The estimated value of the effective absorber thickness T_a for single line PM spectra was about 4.5 ($T_a = f_a n_a \sigma_0$, where n_a is the number of ^{119}Sn atoms per m^2 in the absorber and σ_0 is the resonant cross-section for nuclear γ-ray transition) and it was at least four times larger than for the low temperature FM spectra. One can suppose that possibly the unexpected shift between FM and PM states is due to not completely corrected absorber thickness effect and not to a real change of the amplitude $<u^2>$ of ^{119}Sn atoms. Surprisingly, no anomaly at T_{M-I} was found in the temperature dependence of the $-\ln(f/f_0)$ parameter.

Above T_C, the Mössbauer spectrum consists of the "single" absorption line and was fitted with a quadrupole doublet. The obtained isomer shift parameters showed typical values of Sn^{+4} of about 0 mm/s (the IS values are given relative to a $Ba^{119}SnO_3$ source kept at *RT*), while the small quadrupole splitting QS values indicate the orthorhombic distortion of the ideal perovskite structure. The temperature variation of the calculated QS, Γ (= $\Gamma_s + \Gamma_a$) and IS parameters is shown in Fig. 6. The IS shows a normal linear increase with decreasing temperature. The QS and Γ shows nonlinear increase with decreasing temperature indicating that the magnitude and variance of local distortions are also nonlinearly increasing towards T_C temperature.

In order to obtain reliable distribution of the static hyperfine field B_{hf} for the low temperature FM phase, where the PM like and FM contributions appear to coexist, a different fitting procedure was applied. In the preliminary step, the refined, by the described above method, PM like contribution was subtracted from the spectrum. Next, the fitting program based on the method developed by Hesse *et al.* [6] and by Le Caer *et al.* [9] was applied to determine the distributions of the B_{hf} in the spectra. The hyperfine field distribution functions $P(B_{hf})$ obtained from the spectra measured at different temperatures are shown in Fig. 7. It is seen that already at 15 K, a considerable asymmetric distribution of B_{hf} takes place. With increasing temperature

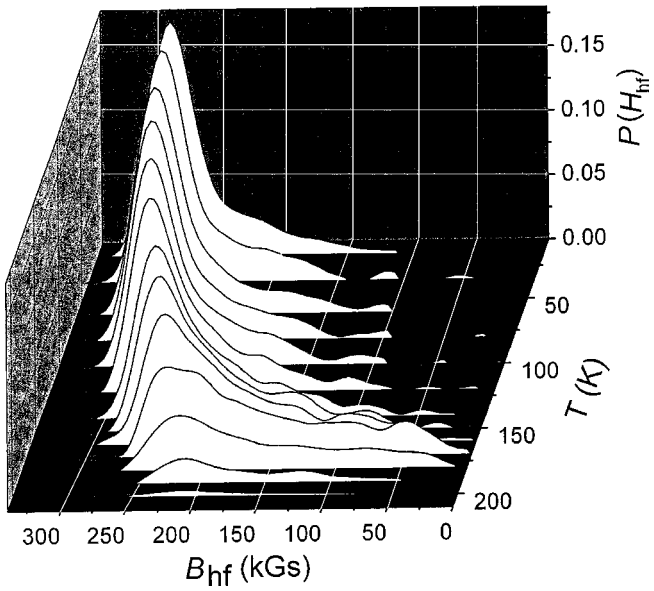

Fig. 7. Temperature dependence of hyperfine field distribution $P(B_{hf})$.

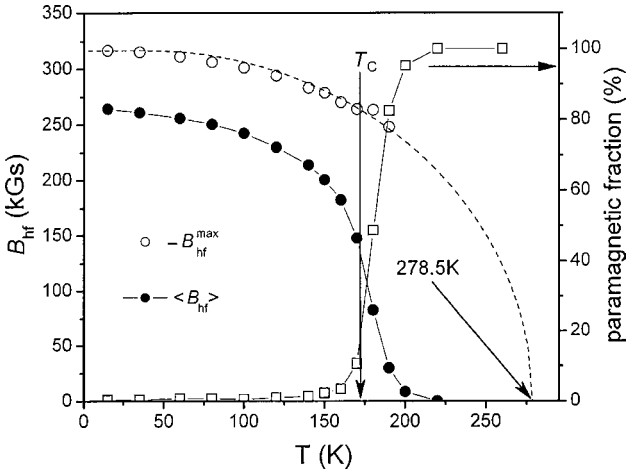

Fig. 8. Temperature dependence of the PM component and $<B_{hf}>$ and B_{hf}^{max} values of the hyperfine field distribution. Dashed curve corresponds to the molecular field theory for $S = 1.83$. Solid lines are to guide the eyes.

the spread of this distribution is slowly growing at the expense of the maximum of the $P(B_{hf})$. The maximal B_{hf}^{max} and mean $<B_{hf}>$ values of the hyperfine field distributions, together with the relative amount of the PM fraction, were plotted as a function of temperature in Fig. 8. The PM contribution, denoted by empty squares (□) in Fig. 8, was taken into account in the calculation of $<B_{hf}>$. The $<B_{hf}>$ points shows quite a normal temperature dependence resembling the M(T) curves. There is a much weaker temperature dependence of B_{hf}^{max} which still has above T_C (at 190 K) about 78% of its lowest temperature value. One should note that some PM contribution appears at about 150 K and that its amount sharply increases at temperatures higher than 160 K. This transition was finished at about 200 K and at temperatures higher than 200 K only the PM phase was found. The theoretical dashed curve fitted to B_{hf}^{max} points is based on the molecular field theory applied to mixed-valent $Mn^{3.33+}$ with spin value $S = 1.83$ and gives $T_C^* = 278.5$ K (as indicated by the arrow). From the T_C value, one can estimate the strength of the Mn-Mn double exchange interaction $J_{Mn\text{-}Mn} = 13.4$ K = 1.16 meV ($J_{Mn\text{-}Mn} = \{3T_C^*/2nS(S+1)\}$ [8]).

Discussion and conclusions

Our Mössbauer and XRD results confirmed that single phase $(La_{0.67}Ca_{0.33})(Mn_{0.99}{}^{119}Sn_{0.01})O_3$ was formed (sample #2) and that all Sn^{4+} cations replace exclusively Mn^{4+}. The Sn doping causes an increase of Mn^{3+}/Mn^{4+} ratio, and reduces the number of available hopping sites for electrons. The Sn^{4+} cations cannot be coupled magnetically to manganese, so that neither ferromagnetism nor metallicity can be generated by such cations. In this sense, Sn substitution should cause similar effects to Fe substitution. In addition, due to their larger size, Sn^{4+} cations introduce local lattice distortions which slow down the electron hopping, and as a result, lead to a stronger suppression of T_C and $T_{M\text{-}I}$. These expectations were confirmed by the results of magnetic measurements presented in Fig. 2, which revealed rather low T_C value as compared to T_C = 166 K for $(La_{0.6}Ca_{0.3})(Mn_{1-x}Fe_x)O_3$ compound with $x = 0.04$ [10]. The resistivity measurements on undoped $(La_{0.67}Ca_{0.33})MnO_3$ usually show that $T_{M\text{-}I}$ temperature (245 K, defined as the maximum in R(T) curve) practically coincides with T_C (246 K, defined as the minimum of dM/dT) [10]. The 66 K difference between T_C and $T_{M\text{-}I}$ obtained for Sn doped sample shows a stronger effect than the Fe doping ($T_C - T_{M\text{-}I} = 46$ K) which was found for $(La_{0.6}Ca_{0.3})(Mn_{0.94}Fe_{0.06})O_3$ compound [10]. These results clearly show that transition from FM metal to PM insulator in $(La_{0.67}Ca_{0.33})(Mn_{0.99}{}^{119}Sn_{0.01})O_3$ goes via FM insulator. It should be noted, from Figs. 5 and 8 that T_C seen by Mössbauer spectroscopy is distinctly higher than the one obtained from magnetization measurement.

The observed huge separation of T_C and $T_{M\text{-}I}$ was a very fortunate case in our Mössbauer study of the temperature dependence of $-\ln(f/f_0)$ parameter. Due to this, clearly no anomaly of $-\ln(f/f_0)$ at $T_{M\text{-}I}$ and a rather spurious increase around T_C, due to saturation effect, was found (Fig. 5). At present, it is not completely clear how to interpret this result. The $-\ln(f/f_0)$ parameter has the sense of the ($<u^2> - <u_0^2>$) and gives information about the stiffness of Mn sublattice. One can emphasize the difference in meaning of Mössbauer $<u^2>$ which is probing dynamics of Mn sublattice and $<u^2>$ from X-ray/neutron diffraction or EXAFS which are additionally sensitive to static displacements of atoms or one can consider the fact that measurements are done on foreign, heavier and larger Sn atoms embedded in Mn sublattice.

To interpret temperature evolution of Mössbauer spectra, one should note from Fig. 4 that they practically preserve the 15 K shape up to about 150 K. Due to this they should be analyzed in terms of static distribution of B_{hf}. For $T \geq 150$ K coexistence of FM and PM phases is evident from the shape of Mössbauer spectra indicating the inhomogeneous character of the transition. But even in this temperature range it is reasonable to assume the existence of static component of the spectra corresponding to the B_{hf}^{max} (NMR measurements on a series of $Ln_{0.67}Ca_{0.33}MnO_3$ compounds showing that long lived ferromagnetic clusters of double exchange coupled Mn spins can survive at temperatures higher than the magnetic ordering temperature obtained from magnetization measurements [7]). The presence of PM line in Mössbauer spectra is due to dynamic phase separation, i.e. coexistence of small FM domains (clusters) undergoing superparamagnetic like relaxation and small PM insulating clusters in the vicinity of T_C. This reasoning shows that temperature evolution of B_{hf}^{max} has more direct and simple interpretation than $<B_{hf}>$ which is possibly influenced by superparamagnetic relaxation effects. By fitting the theoretical function, based on the molecular field theory to experimental values of B_{hf}^{max} (Fig. 8), the value of the T_C^* (≈ 280 K) for Mn moments inside the FM domains was obtained. It is much higher than the T_C (172 K) obtained from magnetization measurement, which should rather be called the blocking temperature, if the relaxation process observed is approximated with superparamagnetic relaxation.

References

1. Billinge SJL, Proffen Th, Petkov V, Sarrao JL, Kycia S (2000) Evidence for charge localization in the ferromagnetic phase

of $La_{1-x}Ca_xMnO_3$ from high real-space-resolution X-ray diffraction. Phys Rev B 62:1203–1211
2. Booth CH, Bridges F, Kwei GH, Lawrence JM, Cornelius AL, Neumeier JJ (1998) Lattice effects in $La_{1-x}Ca_xMnO_3$ ($x = 0 \rightarrow 1$): relationships between distortions, charge distribution and magnetism. Phys Rev B 57:10440–10454
3. Chechersky V, Nomura K, Nath A, Ju H, Green RL (1997) Emission Mössbauer study of CMR manganite $La_{0.8}Ca_{0.2}MnO_3$. II. Step-by-step snapshots of the metal-insulator transition. Low Temp Phys 23:549–553
4. Dagotto E, Hotta T, Moreo A (2001) Colossal magnetoresistant materials: the key role of phase separation. Phys Rep 344:1–153
5. Dai P, Zhang J, Mook HA, Liou S-H, Dowben PA, Plumer EW (1996) Experimental evidence for the dynamic Jahn-Teller effect in $La_{0.65}Ca_{0.35}MnO_3$. Phys Rev B 54:R3694–R3697
6. Hesse J, Rübartsch A (1974) Model independent evaluation of overlapped Mössbauer spectra. J Phys E: Sci Instrum 7:526–532
7. Kapusta Cz, Riedi PC (1999) NMR spectroscopy in mixed valence manganites. J Magn Magn Mater 196/197:446–450
8. Kittel Ch (1996) Introduction to solid state physics, 7th ed. John Wiley & Sons, New York
9. Le Caer G, Dubois JM (1979) Evaluation of hyperfine parameter distributions from overlapped Mössbauer spectra of amorphous alloys. J Phys E: Sci Instrum 12:1083–1090
10. Rao GH, Sun JR, Kattwinkel A *et al.* (1999) Magnetic, electric and thermal properties of $La_{0.7}Ca_{0.3}Mn_{1-x}Fe_xO_3$ compounds. Physica B 269:379–385
11. Rodriguez-Carvajal J (1993) Recent advances in magnetic structure determination by neutron powder diffraction. Physica B 192:55–69
12. Simopoulos A, Kallias G, Devlin E, Panagiotopoulos I, Pissas M (1998) Spin fluctuations in $La_{2/3}Ca_{1/3}MnO_3$ probed by ^{57}Fe and ^{119}Sn Mössbauer spectroscopy. J Magn Magn Mater 177/181:860–861
13. Zener C (1951) Interaction between the *d*-shells in the transition metals. II. Ferromagnetic compounds of manganese with perovskite structure. Phys Rev 82:403–405
14. Żukrowski J, Przewoźnik J, Japa E, Krop K, Kellner K, Gritzner G (2003) Dynamics of $La_{2/3}Ca_{1/3}MnO_3$ doped with ^{57}Fe. Acta Phys Pol B 34:1521–1526